PAPER

Symmetry-constrained quantum coupling in non-Fermi-liquid transport

To cite this article: Rong Li and Zhen-Su She 2023 *Chinese Phys. B* **32** 067104

Symmetry-constrained quantum coupling in non-Fermi-liquid transport

Rong Li(李荣)[1,2] and Zhen-Su She(佘振苏)[1,†]

[1] *State Key Laboratory for Turbulence and Complex Systems, College of Engineering, Peking University, Beijing* 100871, *China*
[2] *Key Laboratory of Coastal Environment and Resources of Zhejiang Province, School of Engineering, Westlake University, Hangzhou* 310030, *China*

(Received 24 September 2022; revised manuscript received 2 March 2023; accepted manuscript online 3 March 2023)

Finding the common origin of non-Fermi liquids (NFLs) transport in high-temperature superconductors (HTSCs) has proven to be fundamentally challenging due to the prominence of various collective fluctuations. Here, we propose a comprehensive non-Hermitian Hamiltonian (NHH) for quantum coupling of multiple scattering mechanisms associated with four types of order fluctuations. It predicts that the anticommutation symmetry of the spinor fermions constrains the scattering rate to a unified quadrature scaling, i.e., $\Gamma = \Gamma_{\rm I} + \sqrt{\Gamma_{\rm Q}^2 + (\mu k_{\rm B} T)^2 + (\nu \mu_{\rm B} B)^2 + (\gamma_E E)^2}$. This scaling yields a comprehensive and accurate description of two widespread NFL behaviors in HTSCs, i.e., a temperature-scaling crossover between quadratic and linear laws and the quadrature magnetoresistance, validated by several dozens of data sets for broad phase regimes. It reveals that the common origin of these behaviors is the spinor-symmetry-constrained quantum coupling of spin-wave and topological excitations of mesoscopic orders. Finally, we show that this NHH can be easily extended to other complex quantum fluids by specifying the corresponding symmetries. It is concluded that this work uncovers a critical organization principle (i.e., the spinor symmetry) underlying the NFL transport, thus providing a novel theoretical framework to advance the transport theory of correlated electron systems.

Keywords: non-Fermi liquid, non-Hermitian Hamiltonian, anticommutation symmetry, quantum coupling, multiple scattering mechanisms

PACS: 71.10.Hf, 31.30.jy, 11.30.Fs, 75.25.Dk **DOI:** 10.1088/1674-1056/acc0f4

1. Introduction

A characteristic of correlated electron systems, including cuprate and iron-based high-temperature superconductors (HTSC) as well as heavy fermions, is that they are highly susceptible to various symmetry-breaking orders.[1–3] By tuning the transition temperature toward absolute zero, i.e., reaching the so-called quantum critical point (QCP), these orders compete or intertwine with each other.[4,5] Near this QCP, collective fluctuations of order parameters usually result in unconventional metallic states (called non-Fermi liquids, NFLs) with transport and thermodynamic properties[6–8] that are significantly different from those of Landau's Fermi liquid.[9,10] The quantum origin (i.e., the electronic state and scattering mechanism) of this NFL is one of the central conundrums of condensed matter physics due to a lack of theoretical methods that take into account strong quantum fluctuations in the presence of abundant low-energy degrees of freedom.[8]

In this context, two resistivity anomalies recently discovered in both iron-based and cuprate HTSCs and amply discussed are the temperature-scaling crossover[11–17] and an accompanied quadrature magnetoresistance (MR).[17–20] The former reveals a well-known universal temperature (T) vs. doping phase diagram for HTSC metallic states, that is, the zero-field resistivity transfers from low-T quadratic to high-T linear scalings. On the other hand, the latter has quadrature coupling $\sqrt{\alpha^2 T^2 + \beta^2 B^2}$ (α and β are empirical slopes) of temperature and magnetic field (B). These two anomalies are beyond understanding with either one-fold scaling (i.e., T^n, where n is the scaling exponent) or semiclassical linear superposition of different scattering rates or conductivity components.

Explaining the common origin of these accompanying anomalies appears to be a fundamental challenge for the present four classes of NFL transport theory. First, most QCP theories attribute NFL transport to scattering electrons of critical fluctuations of a one-fold order parameter,[7,8] such as spin fluctuations[7,21] and dynamic charge density wave.[22] However, experimental data show that the quadrature MR can exist both near[18] and beyond the QCP[20] of various orders (e.g., antiferromagnetism and nematicity), which indicates the independence of the specific order parameter and challenges one-fold QCP scenarios. Second, disorder-driven NFL theory attributes NFL transport to the interplay of impurities (both quenched and magnetic) and strong electronic correlations.[7,23,24] However, the linear-in-B MR and the linear-in-T resistivity have good similarity, e.g., their corresponding scattering rates ($1/\tau$) are close to the Planckian limits, i.e., $\hbar/\tau \sim k_{\rm B} T$ and $\sim \mu_{\rm B} B$, ($\hbar$, $k_{\rm B}$ and $\mu_{\rm B}$ are the reduced Planck constant, the Boltzmann constant and the Bohr magneton, respectively) for many cuprates and iron-pnictide compounds.[18–20,25] This similarity implies that the

†Corresponding author. E-mail: she@pku.edu.cn

MR may have the same origin as the linear-in-T resistivity,[20] which is closely related to quantum dissipation[26] rather than sample heterogeneity and impurities. Third, beyond the single-particle scenario mentioned above, many-body theories[27–29] are devoted to uncovering collectively entangled quantum states (e.g., quantum chaos,[28] or nanometric turbulent flows[29]) underlying the NFL. These theories have been successful in obtaining linear-in-T and B (with disorder[24]) scalings but not in explaining scaling crossover. Thus, fourth, descriptions of the scaling crossover and quadrature MR data are mainly from phenomenological[30,31] and empirical[18,20] models, most of which are based on semiclassical linear superpositions of different conductivity components, scattering rates, or relaxation times. In conclusion, the existing microscopic and phenomenological theories are partially successful in obtaining either the T-scaling crossover or quadrature MR, and they have not provided a unified interpretation of these two associated anomalies.

This conundrum is rooted in the phase-diagram complexity (i.e., various forms of orders and collective fluctuations) induced by the strong electron–electron correlations, which make the simple methodology aiming to find a universal one-fold microscopic mechanism for NFL impractical.[1] To break through this dilemma, a new trend toward comprehensive theories considering the quantum coupling of multiple degrees of freedom (e.g., intertwined and vestigial orders) is emerging.[4,5] Here, we extend this perspective to NFL transport to address the critical questions of whether and how these two resistivity anomalies share a common quantum origin in the following ways. On the one hand, the corresponding scattering rates of T-linear and B-linear resistivity of the strange metal are close to similar Planckian limits.[18–20,25] Moreover, the quadrature MR shows a crossover from quadratic scaling at low magnetic fields to linear scaling at high magnetic fields,[20] which resembles the T-scaling crossover of zero-field resistivity.[11,14] These similarities suggest a unified picture for transport in varying magnetic fields and temperatures in the HTSC. As with the B-scaling crossover originating from the quadrature coupling of magnetic ($\propto \mu_B B$) and thermal ($\propto k_B T$) energies, the T-scaling crossover at zero fields may originate from a quadrature coupling of thermal energy and an unknown intrinsic energy scale. Therefore, we propose that a common origin exists, and it must involve quantum coupling of at least three transport energy scales. In other words, the missing term for most existing theories is the quantum coupling of multiple scattering mechanisms associated with widespread collective fluctuations of intrinsic orders, e.g., spin, charge, and orbital current orders in HTSCs.[1,4,6,32]

We thus aim to construct a unified framework to calculate this quantum coupling effect in NFL transport. Interestingly, the quadrature coupling of multiple energy scales in the single-particle dispersion can be determined by a straightforward calculation of the mean-field Hermitian Hamiltonian describing the intertwined orders of density wave and superconductivity.[33] Therefore, is an effective Hamiltonian describing the quantum coupling effect in NFL transport? In fact, in the quantum transport theory[34] of weakly coupled electrons, multichannel scattering is generally calculated from an effective non-Hermitian Hamiltonian (NHH).[35] However, applying this microscopic theory to strongly correlated electrons has rarely been successful until recently,[36] owing to the nonperturbed nature of electron–electron interactions. Here, we propose a novel NHH integrated with a symmetry-breaking analysis. This analysis is inspired by a recently successful theory of wall turbulence,[37] which demonstrated that, despite a strong correlation at high Reynolds numbers, the dilation symmetry constrains eddy motions to be self-organized into several (generally 4 to 5) statistical ensembles characterized by definite lengths obeying scaling transitions between different power laws. Therefore, scaling transition or crossover is a standard feature of turbulent motions and is constrained by a fundamental symmetry mechanism. Similarly, macroscopic NFL transport shows simple quadrature coupling and scaling crossover, indicating the integration of numerous microscopic degrees of freedom to yield simple (power-law) behavior of ensemble-averaged scattering rates with a universal coupling mechanism.

This work reports a concise symmetry-constrained NHH to model the quantum coupling of multiple scattering mechanisms in NFLs. Specifically, we first map the transport state of an HTSC to a quantum fluid composed of elementary excitations described by a nonequilibrium wave function with multiple spin components. At the ensemble-average level, the dominant contribution of electron–electron correlations to the transport scattering of these excitations is attributed to four types of collective fluctuations: intrinsic (spin or charge) fluctuations, thermal and magnetic excitations, and electric-field excited fluctuations. Under the anticommutation-symmetry constraint of the spinor fermion, this NHH predicts a unified quadrature coupling formula for the total scattering rate, which resembles the single-particle dispersion of intertwined orders.[33] Subsequently, we show that the coupling of intrinsic spin fluctuations and thermal vortices straightforwardly yields a T-scaling crossover from quadratic to linear laws, validated by resistivity data for dozens of samples of cuprates, iron pnictides, and heavy fermion compounds. These validations have revealed the NFL origin rather than a Fermi liquid for quadratic-in-T resistivity in underdoped HTSCs. Furthermore, by utilizing data for cuprates and iron pnictides, we demonstrate that the quadrature MR originates from the quantum coupling of thermal and magnetic vortices, which must extend beyond the QCP. These findings allow us to conclude

that the quadrature scaling behaviors for NFL transport are mainly determined by spin-dependent multichannel scattering with various spin-wave and topological fluctuations, and the NHH model with a critical organization principle of the spinor symmetry is the most appropriate framework for describing such scattering. Finally, we show that this NHH can be easily extended to other complex quantum fluids (e.g., the newly discovered bosonic strange metal[38] and the coexistence of NFL and Fermi liquid[20]) by specifying the corresponding symmetries. Therefore, complementary to the current Hermitian Hamiltonian theories focusing on the single-particle and thermodynamic properties, the present symmetry-constrained NHH model may provide a novel framework to understand NFL transport in strongly correlated electron systems.

In this work, some acronyms are used to identify the cuprates and iron pnictides, Bi-2212 for $Bi_2Sr_2Y_xCa_{1-x}Cu_2O_8$, Bi-2201 for $Bi_2Sr_{2-x}La_xCuO_{6+\delta}$, Ca-YBCO for $Y_{0.7}Ca_{0.3}Ba_2Cu_3O_{7-\delta}$, LSCO for $La_{2-x}Sr_xCuO_4$, YBCO for $YBa_2Cu_3O_{6+\delta}$, Hg-1201 for $HgBa_2CuO_{4+\delta}$, and BaFeAsP for $BaFe_2(As_{1-x}P_x)_2$.

2. Non-Hermitian quantum dynamics of NFL transport

2.1. An effective dynamical equation for NFL transport

We propose that, in strongly correlated electron systems, various collective fluctuations lead to quantum coupling of multiple scattering mechanisms, which a semiclassical theory cannot describe. The main reason is that the Boltzmann equation describes the evolution of the diagonal elements of the density matrix and thus does not apply to off-diagonal elements of the density matrix characterizing the quantum coupling effect of multiple scattering mechanisms. Therefore, we suggest returning to quantum dynamics in utilizing the NHH[34,35] to describe the dissipation of this NFL transport. Generally, this kind of quantum transport is calculated by linear response theory (i.e., the Kubo formula). However, its application to this work requires considering three symmetry-breaking orders and four types of collective excitations. This involves so many microscopic degrees of freedom that simple analytic and numerical calculations are hard to succeed. To overcome these difficulties, we propose a concise phenomenological approach to extract the crucial degree of freedom. There are two essential steps: first, one needs to specify the nonequilibrium many-body quantum state; then, one needs to calculate the relaxation rate of this state, which requires careful consideration of the quantum coupling effect of multiple scattering channels.

From a macroscopic perspective, charge transport in a metal corresponds to a many-body electronic state with finite total momentum along the electric field direction (as $+z$ conventionally). For fermionic metal, the typical case, this transport state comprises many excited fermions with positive excitation energies relative to Fermi energy. In an open-quantum-systems view, we can consider the transporting excitations as a quantum system and the underlying lattice as an environment, respectively. In this case, as with the NHH dynamics of open quantum systems and its recent extension to single-particle excitation of the equilibrium state in strongly correlated electron systems,[36] we propose that quantum dissipation of the nonequilibrium excitations can be represented by a Schrödinger equation with an effective NHH, as follows (ansatz No. 1, the NHH dynamics of nonequilibrium excitations):

$$\mathrm{i}\hbar\frac{\partial}{\partial t}|\Psi_1\rangle = \left(\hat{H}_0 + \mathrm{i}\hat{H}_\mathrm{D}\right)|\Psi_1\rangle, \tag{1}$$

where $|\Psi_1\rangle$ represents the wave function of the nonequilibrium excitation, $\hat{H}_0 = \sum_{\sigma,\varepsilon}\varepsilon c^\dagger_{\varepsilon,\sigma}c_{\varepsilon,\sigma}$ is the conventional Hermitian Hamiltonian, $c_{\varepsilon,\sigma}$ represents the single-particle eigenstate resulting from both the periodic potential and electron–electron interactions, ε is the energy, spin σ and $\sigma' = \uparrow$ or $\downarrow$, and $\mathrm{i}\hat{H}_\mathrm{D}$ is the anti-Hermitian part representing decay due to various scattering by disordered fluctuations.

Generally, $|\Psi_1\rangle$ involves numerous microscopic momentum states. However, the temperature scaling transition and the quadrature magnetoresistance considered in this work are universal behaviors of cuprates, iron-based superconductors, and heavy fermion materials. At the same time, the Fermi surface and its momentum dependence have significant differences in orbitals, gap symmetry, and dimensions among these materials.[1,2,39] Thus, the highly specialized momentum dependence may be less relevant to these two universal transport scalings discussed in this work. This conclusion is especially reasonable for the strange metal phase since the linear-in-T Planckian scattering rate is isotropic and may emerge from momentum-independent inelastic scattering.[40] Therefore, in this work, we choose to deal with the momentum-averaged scattering rate to calculate the transport coefficients from its temperature, magnetic field, and energy dependence.

2.2. Scattering matrices associated with multiple spin channels

On the other hand, unlike simple metals, strongly correlated electron systems (such as cuprates, iron pnictides, and heavy fermion compounds) have a strong correlation that may be closely related to the electron spin, which strongly affects the ordered (e.g., antiferromagnetism and superconductivity) phases and transport properties. Therefore, we believe spin correlation is most relevant to NFL transport in HTSCs. Thus, as the first step towards a comprehensive theory, one should focus on evaluating the transformation of spin states responses

to scattering by collective fluctuations (ansatz No. 2, spin-scattering dominance).

In this case, Eq. (1) describes the decay dynamics of the nonequilibrium excited states under multichannel spin scattering described by $\hat{H}_{\rm D}$, whose quantification is the central object of this section. It is well known that HTSCs show unprecedented prominence of various forms of collective fluctuations,[1] which result in significant scattering and complex dissipation. However, we only concern with the normal phase of these HTSCs so that we can neglect the superconducting fluctuations. In this case, according to different sources (intrinsic or extrinsic), we classify scattering mechanisms into five categories, namely, intrinsic quantum fluctuations (e.g., spin or charge fluctuations[32,41,42]), structural disorder (such as nonmagnetic impurities), thermally excited collective fluctuations (e.g., thermal vortices[25,43]), collective fluctuations excited by magnetic fields (e.g., magnetic vortices[25]), and collective fluctuations associated with electronic fields.

As a concrete example (neglecting phonons and magnetic impurities to highlight the contributions of collective electronic excitations), we study here the specific scattering mechanism for the cuprate HTSC to specify the anti-Hermitian operator matrix $\mathrm{i}\hat{H}_{\rm D}$. As shown in Fig. 1, for the pseudogap and strange metal phases of cuprates, there are four types of collective fluctuations: fluctuations of intrinsic density wave order (DWO, either spin or charge),[44] magnetic and thermal vortices,[25] and instantons.[43] They are typical spin-wave and topological excitations of spin, charge, and current orders (quantum eddies), which were demonstrated by Varma[6,43] and us[25,44] to be the crucial origin of the cuprate NFL. Specifically, the quasistatic spin or charge DWO emerges at low temperatures to reconstruct the Fermi surface into electron pockets,[45] but their dynamical fluctuations are observed to pervade the T–B–doping phase diagram of cuprate HTSCs.[46,47] In contrast, the linear resistivity of the strange metal mainly occurring at high temperature or strong fields[17–19,48,49] is originated from topological vortices excited by thermal fluctuations or magnetic fields. These magnetic and thermal vortices are mesoscopic excitations (cyclotron motions of normal carriers rather than Cooper pairs) of the loop current order[43] rather than the superconducting order, and have distorted array structure of vortices and spatially staggered distribution of vortex, and antivortex,[25] respectively. These are the dominant fluctuations of the intertwined orders in the normal state of cuprate HTSC. Therefore, to comprehensively describe NFL transport, we express $\hat{H}_{\rm D}$ as a linear superposition of five scattering matrices, one for each scattering mechanism

$$\hat{H}_{\rm D} = \hat{D}_{\rm I} + \hat{D}_{\rm Q} + \hat{D}_T + \hat{D}_B + \hat{D}_E, \tag{2}$$

where $\hat{D}_{\rm I}$ is the Hermitian scattering matrix of nonmagnetic impurity scattering, while the last four terms on the right-hand side are the Hermitian scattering matrices associated with collective fluctuations of intrinsic spin or charge fluctuations (i.e., DWO), thermal and magnetic vortices, and electronic-field excited instantons, respectively.

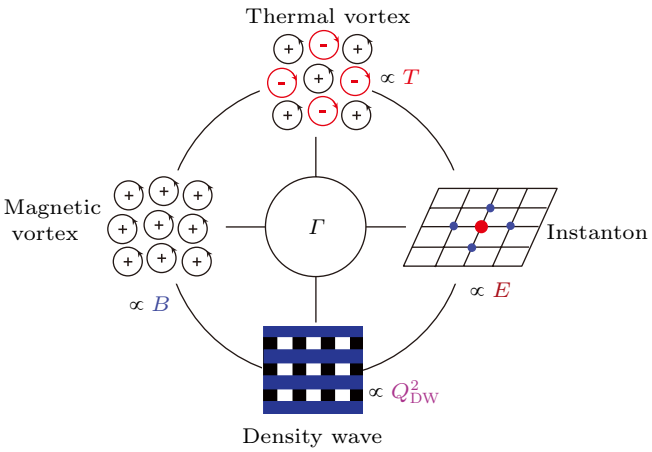

Fig. 1. Four types of collective excitations in cuprate HTSCs. The checkerboard (it could be stripe instead) pattern represents the spin (or charge) density wave order (DWO) and fluctuations,[41,42] determining quadratic scaling of the scattering rate with the DWO wave vector.[44] The magnetic and thermal vortices are mesoscopic topological excitations (i.e., some kinds of quantum eddies) of normal loop currents[43] rather than the cyclical supercurrent of the superconducting order, which determine the linear scalings of the scattering rate with magnetic field and temperature in the strange metal phase.[25] The instanton excitations have a phase jump of $\pm 2\pi$ in a time step at a given point in space[43] and are assumed to determine linear scaling of the scattering rate with energy.

We model these scattering matrices through a symmetry analysis described here. First, it is easy to specify $\hat{D}_{\rm I} = -\Gamma_{\rm I}\hat{I}$, since nonmagnetic impurity scattering is independent of spin configurations, where $\Gamma_{\rm I}$ is the scattering rate independent of temperature and magnetic field. Similar to $\hat{D}_{\rm I}$, we can describe each other scattering matrix in Eq. (2) as the product of a scattering rate and a four-by-four matrix

$$\hat{D}_j = -\Gamma_j \hat{K}_j, \tag{3}$$

where Γ_j ($j = {\rm Q}, T, B,$ or E) is the real characteristic scattering rates of each scattering channel, and $\hat{K}_j$ is the corresponding Hermitian ($\hat{K}_j^\dagger = \hat{K}_j$) and unitary ($\hat{K}_j\hat{K}_j^\dagger = \hat{I}$) scattering matrix.

In our recent work,[25,44] it has been demonstrated that scattering by DWO and vortex fluctuations satisfies a unified energy law; namely, the scattering rate energy exhibits quadratic scaling with the reciprocal of the characteristic length ($l_{\rm o}$) for the fluctuating order

$$\Gamma_{\rm o} = \gamma_{\rm o}\frac{h^2}{m^* l_{\rm o}^2}, \tag{4}$$

where $\gamma_{\rm o}$ is a dimensionless scattering coefficient proportional to the module square of the carrier-order coupling. m^* is the effective mass of a carrier. Equation (4) is a natural result of the Umklapp scattering theory under the slight momentum difference and a long-wavelength approximation for the carrier-phason scattering.[25,44] For DWO, $l_{\rm o} = l_{\rm DW}$ is the period

of spin or charge DWO; thus, $\Gamma_{\rm Q} = \pi\gamma^*_{\rm DW}\hbar^2/m^* l^2_{\rm DW}$, where $\gamma^*_{\rm DW} = 4\pi\gamma_{\rm DW}$ is the renormalized scattering coefficient associated with DWO fluctuations (we define $\gamma^*_{\rm o} = 4\pi\gamma_{\rm o}$). For thermal vortex excitation, $l_{\rm o} = 2\hbar/\sqrt{m^* k_{\rm B} T}$ is the reduced thermal de Broglie wavelength; thus, $\Gamma_T = (\pi/4)\,\gamma^*_{\rm TV} k_{\rm B} T$, where $\gamma^*_{\rm TV}$ is the scattering coefficient associated with the thermal vortex. For magnetic vortex excitation, $l_{\rm o} = 2\sqrt{2\hbar/eB}$ is the reduced magnetic length; thus, $\Gamma_B = (\pi/4)\,\gamma^*_{\rm MV}(m_{\rm e}/m^*)\mu_{\rm B} B$, where $\gamma^*_{\rm MV}$ is the scattering coefficient associated with the magnetic vortex. These linear-in-T and linear-in-B dependencies are supported by ARPES[48] or resistivity[18–20] observations.

Finally, we consider the scattering associated with the instanton. According to the Varma's theory,[43] the instanton and anti-instanton have a phase jump of $\pm 2\pi$ in a time step at a given point in space and are equivalent to the generation of a monopole with a charge ± 4 surrounded by four anti-monopoles with charges ∓ 1 as neighbors.[43] Moreover, following the ARPES observations[48] and Varma's calculation of the vertex coupling of instantons to fermions,[43] we assume its characteristic scattering rate is linear-in energy of the nonequilibrium excitation, i.e., $\Gamma_E = \gamma_E E$, where γ_E is the dimensionless scattering coefficient.

2.3. Unified quadrature scaling for dissipation rate and resistivity

In this section, we calculate the total scattering rate determined by the eigenvalue of the scattering matrix $\mathrm{i}\hat{H}_{\rm D}$. Generally, one should calculate the specific elements of $\hat{K}_j$ for each spin-scattering mechanism, which is severely restricted by strong microscopic correlations. Fortunately, we find that, for some fundamental symmetries (e.g., the anticommutation relation of spinor fermions), the eigenvalue of $\hat{D}$ can be obtained through a global symmetry analysis of $\hat{K}_j$, without any calculations about their specific elements. Specifically, the nonequilibrium excitation $|\Psi_{\rm I}\rangle$ has multiple spin components, which is reminiscent of the Dirac wave function for massless spin-1/2 fermions.[50] Furthermore, similar to the magnetic impurity, the spin fluctuations, thermal and magnetic vortices have local magnetic moments inducing spin dependent scattering for carriers, revealing that the scattering mechanism associated with collective fluctuations in HTSCs is highly spin-dependent. Therefore, similar to the spinor matrices of energy and momentum terms in the Dirac equation,[50] we assume that the four scattering matrices for collective fluctuations in Eq. (3) are anticommutative (ansatz No. 3, anticommutation symmetry)

$$\frac{1}{2}\left(\hat{K}_j\hat{K}_k + \hat{K}_k\hat{K}_j\right) = \delta_{jk}\hat{I}, \tag{5}$$

where δ_{jk} is the Kronecker delta function.

Let us discuss the simplest case (of the scattering matrices) in which the nonequilibrium excitation is a spin-1/2 fermionic excitation containing only two spin components. In this case, the fluctuations of antiferromagnetic spin-density waves can lead to spin-flip scattering of this fermionic excitation. On the other hand, the vortex and antivortex of the thermal vortices are spatially staggered, similar to antiferromagnetic spin-density waves, and thus can also cause spin-flip scattering. Since the angular momenta of these two fluctuations (i.e., antiferromagnetic fluctuations and thermal vortices) are spin and orbital types, respectively, their scattering channels are likely to be orthogonal. Thus, for spin-1/2 fermionic excitation, the scattering matrices of these two types of spin-flip scattering will likely correspond to σ_x and σ_y. Furthermore, the scattering of spin-1/2 fermionic excitation by a magnetic vortex is strongly spin-dependent due to the polarized angular momentum (along the direction of the magnetic field) of the magnetic vortex. Therefore, the spin-dependent part of the scattering matrix of the magnetic vortices corresponds to σ_z. Thus, in this simplest and ideal case, the scattering matrices of these three scattering mechanisms satisfy the anticommutation relations of Eq. (5). While in reality, the nonequilibrium excitations of strongly correlated materials contain a large number of particles and spin components, so the scattering matrices must be high-dimensional and complex. However, as long as these scattering matrices satisfy the anticommutation relation of Eq. (5), their scattering rates must be coupled in a quadrature form.

Specifically, to calculate the eigenvalue $\mathscr{E}$ of the total matrix $\hat{H} = E\hat{I} + \mathrm{i}\hat{D}$, we solve the zero determinant equation: $\det[(E-\mathscr{E})\hat{I} + \mathrm{i}\hat{D}] = 0$. Furthermore, the product rule for the determinant ensures that $\det\{[(E-\mathscr{E})\hat{I} + \mathrm{i}\hat{D}]^2\} = 0$. In this context, as shown in Section I A of supplementary material, the anticommutation of the scattering matrix Eq. (5) straightforwardly determines quadrature coupling of multiple scattering channels in the eigenvalues as follows:

$$\mathscr{E}_\pm = E - \mathrm{i}\Gamma_{\rm I} \pm \mathrm{i}\sqrt{\Gamma_{\rm Q}^2 + \Gamma_T^2 + \Gamma_B^2 + \Gamma_E^2}, \tag{6}$$

where $\mathscr{E}_+ = E - \mathrm{i}\Gamma_{\rm I} + \mathrm{i}\Gamma_{\rm a}$ ($\Gamma_{\rm a} \equiv \sqrt{\Gamma_{\rm Q}^2 + \Gamma_T^2 + \Gamma_B^2 + \Gamma_E^2}$) represents acceleration processes (i.e., amplification with $|\phi(t)|^2 = \exp[2(\Gamma_{\rm a} - \Gamma_{\rm I})t]\,|\phi(0)|^2$), while $\mathscr{E}_- = E - \mathrm{i}\Gamma_{\rm I} - \mathrm{i}\Gamma_{\rm a}$ represents dissipation processes with $|\phi(t)|^2 = \exp[-2(\Gamma_{\rm I} + \Gamma_{\rm a})t]\,|\phi(0)|^2$. Relaxation from the nonequilibrium state to the equilibrium state is a dissipation process. Hence, the mean relaxation time of the NFL should be

$$\begin{aligned}\frac{\hbar}{2\tau} &= \Gamma(T,B,E)\\ &= \Gamma_{\rm I} + \sqrt{\Gamma_{\rm Q}^2 + (\mu k_{\rm B} T)^2 + (\nu\mu_{\rm B} B)^2 + (\gamma_E E)^2},\end{aligned} \tag{7}$$

where $\mu = \pi\gamma^*_{\rm TV}/4$ and $\nu = (\pi\gamma^*_{\rm MV}/4)(m_{\rm e}/m^*)$.

Correspondingly, the DC resistivity is determined by elementary excitations on the Fermi surface with $E = 0$. Therefore, by substituting the corresponding relaxation time $\tau =$

$\hbar/(2\Gamma)$ into the Drude model, i.e., $\rho = m^*/n_c e^2\tau$, we predict the DC resistivity for multichannel scattering

$$\rho(T,B) = \rho_I + \sqrt{\rho_Q^2 + \alpha^2 T^2 + \beta^2 B^2}, \tag{8}$$

where $\rho_I = 2\Gamma_I m^*/(\hbar n_c e^2)$ and $\rho_Q = \gamma_{DW}^* R_Q/(n_c l_{DW}^2)$ are the characteristic resistivities associated with simple impurity and DWO fluctuations, respectively, and $R_Q = h/e^2$ is the resistance quantum. In addition, $\alpha = (\pi/2)\gamma_{TV}^* k_B m^*/(n_c e^2\hbar)$ and $\beta = (\pi/4)\gamma_{MV}^* n_c e$ represent the slopes of temperature and magnetic field dependence, respectively, and the carrier density $n_c = pN/(a_0 b_0 c_0)$, where a_0 and b_0 are in-plane lattice constants, c_0 is the c-axis lattice constant, N is the number of Cu or Fe ions on the conducting plane in one unit cell, and p is the effective carrier concentration per ion.

Equations (7) and (8) are the most important results of the present work; these equations indicate that the NFL scattering rate and DC resistivity have a unified quadrature coupling of temperature, magnetic field, energy, and the DWO scattering rate. Note that various empirical and phenomenological quadrature models (e.g., Hayes' quadrature MR model[18] and Varma's quadrature scattering rate model[51]) are asymptotic approximations of our theory at the $\Gamma_{DW} = 0$ limit. However, recent experiments reveal that the DWO is important, especially in the underdoped regime.[1,42] Taking this DWO scattering into account, Eqs. (7) and (8) provide a straightforward unified explanation for various experimentally observed NFL transport behaviors, including the scaling crossover from T^2 to T of zero-field DC resistivity ($B = 0$ and $E = 0$),[11,12,14–16] the quadrature MR $\rho = \sqrt{\alpha^2 T^2 + \beta^2 B^2}$ near a QCP ($\rho_Q \to 0$ and $E = 0$),[17–20] and the quadrature scattering rate $\Gamma = \Gamma_I + \sqrt{(\mu k_B T)^2 + (\gamma_E E)^2}$[48] at ($\rho_Q \to 0$ and $B = 0$). It is worth mentioning that $\rho_Q \to 0$ near a QCP is due to the neglect of the temperature-dependent contribution of spin-wave-like density wave excitations. In this case, the contributions of the density wave excitations to the total scattering rate and resistivity are only determined by the intrinsic energy scale. Since the intrinsic energy scale is lacking at the QCP, Γ_Q and ρ_Q tend to be zero.

In summary, our model is based on general symmetry considerations, i.e., the three aspects of NHH dynamics of nonequilibrium excitation, spin-correlation dominance, and anticommutation symmetry, which are indeed widespread in strongly correlated materials (see also discussion in Section 5). Therefore, the simple quantum coupling indicated in Eqs. (7) and (8) would be universal for NFL transport of various strongly correlated materials. The following two sections verify the quadrature scalings in Eq. (8) with normal-state resistivity data for cuprates, iron pnictides, and heavy fermion compounds. These verifications enable us to determine the scattering coefficients, i.e., γ_{DW}^*, γ_{TV}^*, and γ_{MV}^*, for various order fluctuations to clarify the specific underlying quantum origin of the scaling crossover and the quadrature MR of HTSCs. Since the low-temperature Hall coefficient is approximately T-independent and is thus a good measure of the doped carrier density at not too high doping,[52] and the low-energy effective mass is approximately temperature and doping independent in zero magnetic fields,[53] we assume that the carrier density and effective mass of one sample are T and B independent constants in this work.

3. Quantum coupling origin of temperature scaling crossover

It is widely observed that for cuprates and iron-based HTSCs, the temperature scaling exponent of the zero-field resistivity presents a puzzling continuous variation between 2 and 1 as the temperature changes.[13,14] Considering that orders and fluctuations of these NFL material families are quite different, it is challenging to understand the common origin of these scaling crossovers. However, at a statistical mechanical level, Varma demonstrated that the AFM and loop-current order in HTSCs and heavy-fermion compounds could be uniformly mapped to the two-dimensional (2D) XY model.[43] The four types of collective fluctuations shown in Fig. 1 are typical spin-wave and topological excitations of this model. Therefore, we believe that Eqs. (5)–(8) are universal for the normal states of HTSCs and heavy fermions. This section shows that the quadrature scalings in Eq. (8) can provide a unified and quantitative explanation for the scaling crossover behavior and reveal their universal connections to the quantum coupling effects of order fluctuations.

3.1. Quantum coupling of AFM fluctuations and thermal vortices

In normal states of underdoped cuprates, a sequence of symmetry breaks occur with increasing temperature and generate varying orders,[1] including density wave and nematicity in the pseudogap phase and vortex fluctuations[6,25] in the strange metal phase. It was recently demonstrated theoretically that a partially melted unidirectional DWO (either spin or charge) could generate a vestigial nematic phase,[54] the zero-field resistivity can be considered only with fluctuations of DWO and thermal vortices. In this context, and neglecting impurity scattering for high-quality single crystals, Eq. (8) can be simplified to

$$\rho = \sqrt{\rho_Q^2 + \alpha^2 T^2}, \tag{9}$$

where ρ_Q represents contributions from scattering by the DWO fluctuations.

We first use Eq. (9) to quantify the quantum coupling effects of thermal vortices and AFM spin fluctuations, for which

the order period is $l_{\rm DW} = 2a_0$. It is worth mentioning that to reduce the mathematical complexity of our comprehensive model, we only consider the leading-order contribution of each scattering mechanism. Note that Eq. (9) and our previous study[25,44] reveal that thermal vortices dominate the high-T resistivity, while the DWO fluctuations dominate the low-T resistivity. Furthermore, spectroscopic experiments on the pseudogap phase reveal that the characteristic energies associated with scattering by spin and charge excitations are little affected by the temperature at low T.[46,55] Therefore, the temperature dependence of the spin or charge CDW at high T is secondary and can be neglected. In this case, we choose $\gamma^*_{\rm DW}$ as a constant for mathematical simplicity. In addition, taking the experimentally estimated m^* from Refs. [53,56–58], as well as the carrier density $n_{\rm c}$ estimated with lattice constants and carrier concentration,[16,59,60] we can predict the zero-field resistivity for AFM QCP of cuprate and iron pnictides with Eq. (9), as shown in Fig. 2.

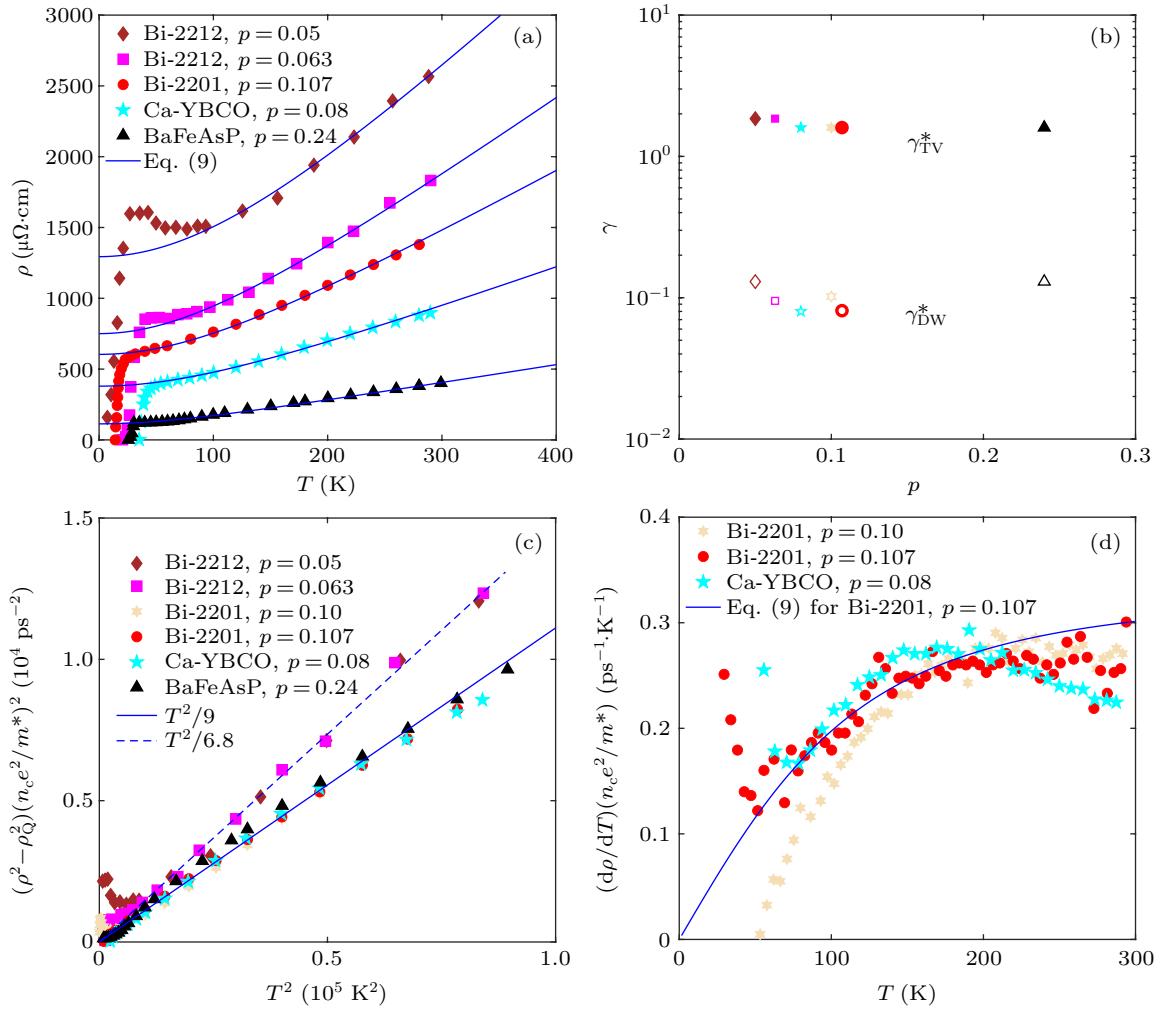

Fig. 2. (a) Zero-field ρ versus T near the AFM QCP. Symbols represent samples near the AFM QCP for various cuprate[61–63] and pnictide[16] compounds. Blue solid lines are predictions for Eq. (9) with $l_{\rm DW} = 2a_0$, carrier density $n_{\rm c} = pN/(a_0b_0c_0)$ estimated with lattice constants and carrier concentration,[16,59,62] effective mass m^* determined from Refs. [53,56–58], and two fitting parameters $\gamma^*_{\rm DW}$ and $\gamma^*_{\rm TV}$. These two fitting parameters are represented by hollow and solid symbols in panel (b), respectively, where p is the concentration of doped carriers. Different colors mark compounds as in panel (a). The wheat symbols represent Bi-2201 at $p = 0.10$. (c) Scaling plot of ρ^2 curves from the samples in panels (a) and (b). After subtracting the contribution of AFM fluctuations, the remainder is multiplied by $\left(n_{\rm c}e^2/m^*\right)^2$. (d) Crossover of the derivative $\mathrm{d}\rho/\mathrm{d}T$. Specific values of parameters are listed in Table 2 in the supplementary material.

This description presents three nontrivial outcomes. First, Fig. 2(a) shows that the fit to the data with most samples is quite satisfactory for accurately capturing the scaling crossover between 30 K and 300 K, although there are apparent deviations at low temperatures due to the inevitable insulator effect and superconducting fluctuations. This agreement is remarkable for its robustness, with only two tunable scattering coefficients ($\gamma^*_{\rm DW} = 0.08$–0.13 and $\gamma^*_{\rm TV} = 1.6$–1.85) shown in Fig. 2(b), although these compounds have very different $\rho_{\rm Q}$ values and linear slopes.

Second, Eq. (9) predicts universal quadratic temperature scaling for the square of the resistivity, as follows:

$$\rho^2 = \rho_{\rm Q}^2 + \alpha^2 T^2. \tag{10}$$

In the ρ^2–T^2 plot, this scaling presents a linear law, as confirmed in Fig. 2(c), and it cannot be described by conven-

tional one-fold scaling $\rho = \rho_{\rm I} + AT^n$, which would be nonlinear in this plot. More interestingly, we find that the $\rho^2 - \rho_{\rm Q}^2$ data normalized by $\left(n_{\rm c}e^2/m^*\right)^2$ for six samples collapsed to two lines, which reveales that the relaxation time τ_T associated with a thermal-vortex scattering in Bi-2212 (i.e., $\sim 2.6/T$ ps) is slightly lower than those of other compounds (i.e., $\sim 3/T$ ps). This collapse and the close relaxation times confirm the universalities of Eq. (10) and the thermal-vortex scattering strength. In addition, since $l_{\rm DW} = 2a_0$, $\gamma^*_{\rm DW} = 0.11 \pm 0.03$ and $m^*/m_{\rm e} = 2.4 \pm 0.1$ ($m_{\rm e}$ is the electron mass) for the five cuprate samples shown in Fig. 2, their scattering rates $\Gamma_{\rm Q} = \pi\gamma^*_{\rm DW}\hbar^2/m^* l^2_{\rm DW}$ associated with AFM fluctuations must be close. Random impurity scattering also cannot explain this similarity, thus precluding one-fold scaling.

Third, Eq. (9) predicts a straightforward scaling crossover from the low-T quadratic law $\rho \to \rho_{\rm Q} + \alpha^2T^2/\rho_{\rm Q}$ to the high-T linear law $\rho \to \alpha T$ with increasing temperature. It also presents in the crossover of the derivative ${\rm d}\rho/{\rm d}T$ from linear scaling $\alpha^2T/\rho_{\rm Q}$ to constant α, as shown in Fig. 2(d). Therefore, the accurate descriptions and robustness of scattering coefficients shown in Fig. 2 reveal that the scattering mechanism of DWO and thermal vortices and their quantum coupling are universal for the AFM QCP of both cuprate and iron-based HTSCs.

It is interesting to compare the present prediction with previous theories for the Fermi liquid-NFL crossover scenario, e.g., Anderson's hidden Fermi liquid model, $\rho = \rho_{\rm I} + \alpha T^2/(T + W)$.[30,64] Figure 5 in the supplementary material shows that Anderson's model achieves an equal level of agreement as to the fit in Fig. 2(a). However, the fitting values for the effective bandwidth W and linear slope α scatter over 47- and 23-fold for cuprate compounds (also noticed in his early work[30]), while the corresponding scatter for $\gamma^*_{\rm DW}$ and $\gamma^*_{\rm TV}$ in our fits is less than $\pm 24\%$, as shown in Fig. 2(b). Furthermore, scatters for W and α are highly correlated and are found to increase sharply when a few more low-T data points are taken into account; this reflects the redundancy of this model. Physically, Anderson's model considers three scattering channels and predicts a low-T Fermi-liquid resistivity $\rho \to \rho_{\rm I} + \alpha T^2/W$ determined by impurity scattering ($\rho_{\rm I}$) and electron–electron umklapp scattering ($\propto T^2$), which is unrelated to high-T quasiparticle decay ($\propto T$ scaling). In contrast, our two-channel model predicts that the low-T quadratic resistivity $\rho \to \rho_{\rm Q} + \alpha^2T^2/2\rho_{\rm Q}$ originates from the quantum coupling of the residual resistivity from DWO fluctuations and the high-T linear resistivity from thermal vortices, which is overlooked in Anderson's model and other Fermi liquid scenarios.[30,64,65] This quantum coupling mechanism is consistent with numerous observations of intertwined orders of spin or charge DWO and current orders.[1,42,66] We conclude that the most reasonable explanation for scaling crossover of underdoped HTSCs from a quadratic to a linear law is the quantum coupling of DWO fluctuations and thermal-vortex excitations rather than the crossover from a simple Fermi liquid to the NFL.

3.2. Quantum-coupling origin of quadratic resistivity in the cuprate pseudogap phase

For underdoped cuprates, recent measurements revealed two distinct phases with quadratic scaling of resistivity:[11,15,65] a small electron-like pocket induced by CDW-driven Fermi surface (FS) reconstruction at low T (and high magnetic fields) and the arc-like FS in the pseudogap phase at intermediate temperature. For the former, Tabiś *et al.* recently demonstrated that a Fermi liquid theory associated with electron–electron umklapp scattering correctly predicts the quadratic resistivity ($\rho = \rho_{\rm I} + A_2T^2$) in underdoped Hg-1201.[65] However, the quadratic resistivity in the intermediate-T pseudogap phase is approximately forty times smaller than in the low-T reconstructed phase, and that of the prediction with this Fermi liquid theory,[65] thus challenging a simple Fermi liquid explanation. In contrast, our theory's inference is that the pseudogap phase's quadratic resistivity has an NFL origin, i.e., quantum coupling between the scattering channels of DWO fluctuations and thermal vortices. Specifically, Eq. (10) predicts the coefficient of the quadratic resistivity contributed by every Cu–O sheet ($A_{2,\square} = A_2N/c_0$)

$$A_{2,\square} = \frac{\alpha^2 N}{2\rho_{\rm Q}c_0} = \frac{\pi}{16}\frac{(\gamma^*_{\rm TV})^2}{\gamma^*_{\rm DW}}\frac{k_{\rm B}^2 m^{*2} l^2_{\rm DW} a_0^2}{\hbar^3 e^2 p}. \tag{11}$$

The second equality is obtained using $\rho_{\rm Q} = \gamma^*_{\rm DW}R_{\rm Q}/(n_{\rm c}l^2_{\rm DW})$, $n_{\rm c}c_0/N = p/a_0^2$ as well as the linear slope $\alpha = (\pi/2)\gamma^*_{\rm TV}k_{\rm B}m^*/(n_{\rm c}e^2\hbar)$. Applying Eq. (11) to AFM fluctuations and assuming parameters are doping independent for hole-doped cuprates (for mathematical simplicity), we substitute $l_{\rm DW} = 2a_0$, the experimentally observed $m^* = (2.5 \pm 0.4)m_{\rm e}$,[57,67,68] $a_0 = 3.82 \pm 0.06$ Å, $\gamma^*_{\rm TV} = 1.7 \pm 0.4$[25] and $\gamma^*_{\rm DW} = 0.11 \pm 0.03$ (extracted from Ref. [44]) into Eq. (11) and show that

$$A_{2,\square}({\rm AFM}) \approx \frac{0.015 \pm 0.009}{p}. \tag{12}$$

The prediction of Eq. (12) will be shown below to be highly consistent with the experimental values of low-temperature and zero-field quadratic resistivity coefficients in two respects. First, the theoretical prediction of the inverse ratio $A_{2,\square} \propto p^{-1}$ agrees exactly with the experimental observations of a simple resistivity scaling $\rho \propto T^2/p$ for a range of cuprates.[11,15] Second, the magnitude of $A_{2,\square}({\rm AFM})$ predicted from Eq. (12) is consistent with experimental values for various cuprate compounds in underdoped regimes,[11,15,69] as

shown in Fig. 3. The agreement is impressive because the prediction involves no additional parameters and determines the parameters independently from previous measurements or studies. This agreement strongly supports the notion that the pseudogap state is an NFL with intertwined orders.[4]

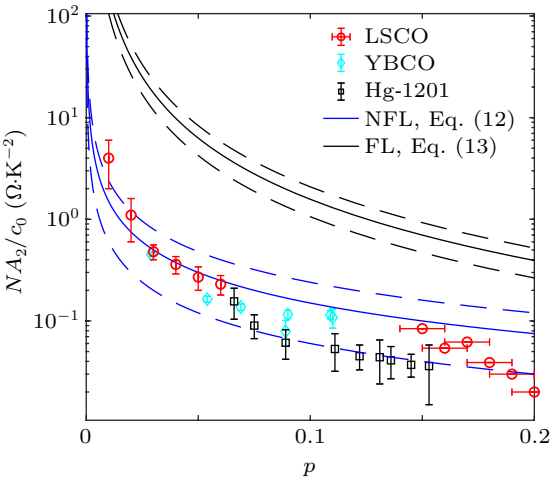

Fig. 3. Quadratic resistivity coefficients $A_{2,\square} = NA_2/c_0$ for undoped cuprates. Here, c_0 is the c-axis lattice constant, and N is the number of Cu ions on the conducting plane in one unit cell. Symbols indicate data of LSCO, YBCO, and Hg-1201, taken from Refs. [11,15,69,70]. The solid and dashed blue lines represent the mean values and error bars for predictions from the NFL model in Eq. (12), respectively. The solid and dashed black lines represent the mean values and error bars for predictions from the Fermi liquid model of Eq. (13), respectively.

On the other hand, it is important to compare our findings with Fermi liquid theory. For a Fermi liquid, $A_{2,\square}$ can be estimated from the expression for the self-energy or scattering rate of electron–electron scattering. In this context, Tabiś *et al.* recently obtained $A_{2,\square}$ for a 2D single-band metal as follows:[65]

$$A_{2,\square}(\mathrm{FL}) = \frac{9\pi^4 k_\mathrm{B}^2}{e^2\hbar^3}\frac{m^{*2}}{k_\mathrm{F}^4} \approx \frac{0.016 \pm 0.006}{p^2}. \tag{13}$$

The second equality originates from the substitution of $k_\mathrm{F}^2 = 2\pi p/a_0^2$ for the 2D tetragonal lattice. In contrast to our theory, the prediction of Eq. (13) is inconsistent with experimental observations for underdoped cuprates in two respects. First, the prediction of an inverse square dependence $A_{2,\square} \propto p^{-2}$ is contrary to experimental observations of simple scaling $\rho \propto T^2/p$.[11,15] Second, the experimentally observed $A_{2,\square}$ for underdoped cuprates is overestimated by one order of magnitude with $A_{2,\square}(\mathrm{FL})$ predicted from Eq. (13), as shown by the solid black line in Fig. 3.

These discrepancies originate from the inverse relationship between the scattering rate $\hbar/\tau_\mathrm{FL} = \left(9\pi^3/4\right) k_\mathrm{B}^2 T^2/E_\mathrm{F}$ and the Fermi energy $E_\mathrm{F} = \hbar^2 k_\mathrm{F}^2/2m^* \propto p$, which is an inevitable result for electron–electron scattering. In contrast, the experimentally observed scaling $\rho \propto T^2/p$ reveals a universal transport scattering rate of $\hbar/\tau = k_\mathrm{B}^2 T^2/E_\mathrm{Q}$, where the characteristic energy E_Q is doping independent over a wide doping range. In this context, our theory (Eq. (7)) correspondingly predicts that $\hbar/\tau = \Gamma_T^2/\Gamma_\mathrm{DW}$ and $E_\mathrm{Q} \approx 0.56\Gamma_\mathrm{DW}$ since $\Gamma_T = (\pi/4)\gamma_\mathrm{TV}^* k_\mathrm{B} T$ and $\gamma_\mathrm{TV}^* \approx 1.7$.[25] Therefore, our theory explains the origin of $\rho = C_2 T^2/p$ with the weakly doping-dependent scattering rates of DWO (for AFM, $\Gamma_\mathrm{DW} = 18 \pm 4$ meV) and thermal vortices ($\Gamma_T = (1.3 \pm 0.3) k_\mathrm{B} T$). Therefore, we conclude that the quadratic resistivity in the intermediate-T pseudogap phase originates from quantum coupling effects of the DWO fluctuations and thermal-vortex excitations rather than electron–electron umklapp scattering. In other words, the pseudogap state is an NFL with intertwined order fluctuations rather than a Fermi liquid, consistent with its arc-like FS and fluctuating DWO, nematicity, and current orders.[1]

In addition, for lightly overdoped cuprates (e.g., Tl-, Y-, Bi-, and La-based compounds), iron pnictides and iron chalcogenides, intrinsic spin (e.g., AFM and ferromagnetic) or charge (e.g., CDW and nematic) fluctuations are still present,[16,46,71–75] although weaker than those in underdoped cases. Thus, the quadratic resistivity in these compounds can be described by our theory. For instance, Fig. 4 in the supplementary material shows that the temperature scaling crossover of zero-field resistivity for iron pnictides (BaFeAsP) and iron chalcogenides ($FeSe_{1-x}S_x$) is well described by Eq. (8). Besides, Eq. (8) also applies to T-scaling crossovers near the ferromagnetic (FM) QCP. As shown in Section II A in the supplementary material, we find that the scaling crossover from quadratic to linear near the FM QCP of $BaCo_2As_2$[76] and the heavy-fermion metals $YbNi_4(P_{1-x}As_x)_2$[77] can be well explained by the quantum coupling of FM and thermal-vortex fluctuations.

4. Quantum coupling origin of quadrature magnetoresistance

In recent years, a quadrature MR of the strange metal phase has been found in both cuprate- and iron-based HTSCs and provides a fundamental challenge for understanding the strange metallicity.[18–20] Especially, Ayres *et al.*[20] observed that the quadrature MR extends well beyond QCP in the overdoped cuprates, i.e., (Pb/La)-doped $Bi_2Sr_2CuO_{6+\delta}$ and $Tl_2Ba_2CuO_{6+\delta}$, which cannot be explained by quantum criticality theory. This finding raises critical questions: first, what is the physical origin of quadrature magnetoresistance, and is it associated with the intertwining of various collective fluctuations? Second, do underdoped cuprates also exhibit a quadrature MR? If so, would spin and charge fluctuations modify the formalism of the quadrature coupling?

The present theory (Eqs. (7) and (8)) provides definite answers to these questions. First, quantum coupling of the spin

scattering channels associated with magnetic and thermal vortices and the DWO fluctuations leads to quadrature scaling of the magnetic field, temperature, and DWO-determined scattering and resistivity in MR. Second, the quadrature MR extends to the underdoped region since vortex excitations are associated with the strange metal in these regimes. This section first demonstrates that the underdoped cuprates exhibit a quadrature MR (Eq. (8)). The additional constant term $\rho_{\rm Q}$ from DW fluctuations reasonably explains the scaling crossover of zero-field resistivity from quadratic to a linear law (as discussed in Section 3). Furthermore, for the quadrature MR near the QCPs, we find a universality for three scattering coefficients, confirming that the quadrature MR originates from the quantum coupling between the scattering channels of three kinds of collective fluctuations.

4.1. Quadrature magnetoresistance in underdoped cuprates

In Bi-2201, at all doping levels marked in Fig. 4(a), the MR at high fields (60 T) exhibits a similar quadratic temperature dependence up to 80 K, revealing possible quadrature coupling of temperature and field. Upon introducing a pseudo temperature scale associated with the quadrature sum of temperature and the field with an appropriate ratio (β/α), i.e., $\tilde{T} = \sqrt{T^2 + (\beta/\alpha)^2 B^2}$, the MR (red) collapses to exhibit the same $\tilde{T}$ dependence as the zero-field resistivity (black) above $T_{\rm sf}$ (the onset temperature of superconducting fluctuations[78]), as shown in Fig. 4(b). Therefore, we have demonstrated that the quadrature MR extends to the underdoped region and is a common feature of strange metals.

Furthermore, Fig. 4 also shows that Eq. (8) without impurity scattering (i.e., $\rho_{\rm I} = 0$) provides a precise description for this feature, including the quadratic temperature dependence of MR in (a) and the transition of quadratic to linear $\tilde{T}$ scaling in (b). The linear scaling at intermediate-$\tilde{T}$ (60 K–100 K) supports quantum coupling between the scattering channels of magnetic and thermal vortices, while the low-$\tilde{T}$ (below 60 K) quadratic scaling is due to further coupling with DWO fluctuations. It is essential to specify the DWO types. At higher doping above the AFM QCP ($p \approx 0.11$), short-range (close to its period) CDW is widespread in Bi-2201.[71] Therefore, we predict that the quadrature MR above $p = 0.11$ should be associated with CDW rather than AFM. Indeed, we find that the MR data for Bi-2201 at $p = 0.12$ can be precisely fitted with the CDW periodicity $l_{\rm CDW} = 3.92a_0$ (the interpolated value of experimental measured data)[71] and the universal scattering coefficient $\gamma^*_{\rm DW} = 0.11$. Furthermore, we find that $\gamma^*_{\rm DW}$ for $p = 0.16$ and 0.18 is much smaller than $p = 0.11$, consistent with experimental observations that the integrated intensity of RXS spectroscopy decreases from $p = 0.12$ to 0.16.[71]

It would be helpful to compare the present analysis (Eq. (8)) with Hayes' empirical formula $\rho(T,B) = \rho_{\rm I} + \sqrt{\alpha^2 T^2 + \beta^2 B^2}$[18] to judge the importance of coupling with DWO fluctuations. For zero-field resistivity, coupling with DWO fluctuations predicts a scaling crossover from quadratic- to linear-scaling, extensively validated by data for cuprates, iron-based HTSCs, and heavy fermion compounds shown in Fig. 2 and Section 2 in the supplementary material. This universal crossover is a nontrivial phenomenon; it is overlooked in Hayes' empirical model predicting a purely linear resistivity $\rho = \rho_{\rm I} + \alpha T$ at zero fields. In contrast, Eq. (8) is a unified description for both the quadrature MR and scaling crossover in cuprate and iron-based HTSCs. Note that Hayes' formula can be derived from Eq. (8) by switching off the DWO channel (i.e., $\Gamma_{\rm DW}$), so we conclude that the missing component for Hayes' formula is the scattering channel of intrinsic low-temperature spin or charge fluctuations.

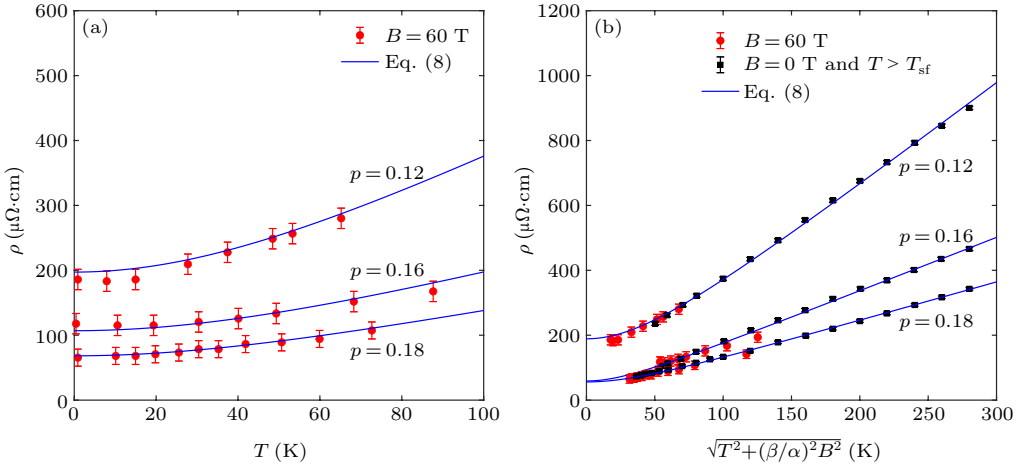

Fig. 4. Quadrature scaling of the in-plane MR in Bi-2201. (a) In-plane MR (red) up to 80 K at 60 T fields for three different hole dopings, i.e., $p = 0.12$, 0.16, and 0.18. (b) MR (red) plotted as a function of $\sqrt{T^2 + (\beta/\alpha)^2 B^2}$ collapses to the same dependence as the zero-field resistivity (black) above the onset temperature ($T_{\rm sf}$) of the superconducting fluctuations.[78] Symbols are data from Ref. [62]. The solid blue lines are predictions from Eq. (8) with the fitting parameters listed in Tables 1 and 2 in the supplementary material.

4.2. Quantum coupling of magnetic and thermal vortices near the QCP

This subsection quantifies the quadrature MR near QCPs and determines corresponding scattering coefficients to verify three inferences from our theory. The first inference is that the MR should be described by Eq. (8) and must collapse to a simple scaling as follows (neglecting impurity scattering near optimal doping):

$$\frac{\rho^2-\rho_{\rm Q}^2}{T^2}=\alpha^2+\beta^2\left(\frac{B}{T}\right)^2. \tag{14}$$

Indeed, Figs. 5(a) and 5(c) show that the MR in wide T (over 100 K) and B (60 T–80 T) ranges for LSCO at the QCP of pseudogap (i.e., $p=0.19$) and BaFeAsP ($x=0.36$) near the AFM QCP ($x=0.31$) are well described by Eq. (8). Moreover, we expect data collapse in wide T and B ranges to the simple scaling of Eq. (14) in Figs. 5(b) and 5(d); however, there are some deviations for low-T data, which may be related to superconductivity or structural transitions, respectively. For the description of BaFeAsP with $x=0.31$ and 0.41, see Section II B in supplementary material.

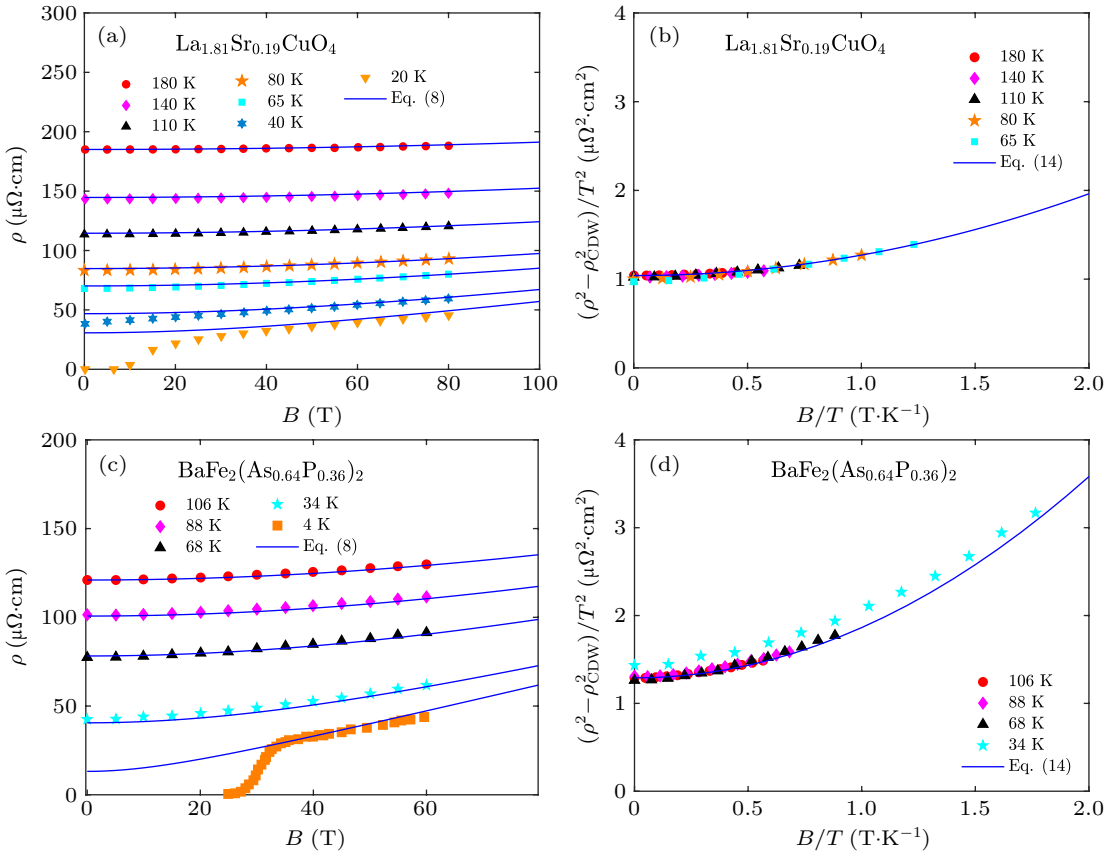

Fig. 5. (a) Field dependence of MR for LSCO with CDW. The symbols represent data for overdoped LSCO ($p=0.19$).[19] Solid lines are predictions from Eq. (8) with $\rho_{\rm I}=0$, experimentally measured (or interpolated) $l_{\rm CDW}=3.92a_0$[79] and $m^*=1.67m_{\rm e}$,[67] as well as tunable parameters $\gamma^*_{\rm DW}=0.039$, $\gamma^*_{\rm TV}=1.67$, and $\gamma^*_{\rm MV}=1.97$. (c) Field dependence of MR for BaFeAsP near the AFM QCP ($x=0.31$). Symbols indicate data for BaFeAsP ($x=0.36$).[18] Solid lines are predictions from Eq. (8) with $\rho_{\rm I}=0$, $l_{\rm DW}=2a_0$, and $m^*=4.65m_{\rm e}$ (estimated from interpolation of experimental data[60,67]), as well as tunable parameters $\gamma^*_{\rm DW}=0.015$, $\gamma^*_{\rm TV}=1.7$, and $\gamma^*_{\rm MV}=7.8$. Panels (b) and (d) exhibit scaling of high-T resistivity for the same data in panel (a) or (c). The solid blue line shows the prediction from Eq. (14) with the same fitting parameters for predictions in panel (a) or (c).

The second inference is that since DWO and their collective fluctuations weaken when doping changes from underdoping to over doping, scattering coefficients associated with these fluctuations should decrease gradually. Indeed, as shown in Table 1, $\gamma^*_{\rm DW}$ for overdoped LSCO ($p=0.19$), optimally doped ($x=0.31$) and overdoped ($x=0.36$ and 0.41) BaFeAsP is less than 0.04, which is much less than the universal value $\gamma^*_{\rm DW}\approx 0.11$ near the underdoped AFM QCP shown in Fig. 2(b). In addition, as discussed in the last subsection, $\gamma^*_{\rm DW}$ for Bi-2201 at $p=0.16$ and 0.18 is smaller than that at $p=0.11$. These observations indicate that the strengths for AFM and CDW fluctuations may remain universal in the underdoped regime but may be suppressed in the overdoped regime, consistent with the reduction (e.g., RXS peak intensity) of the DWO in the overdoped regime.[80]

Thirdly, our previous study pointed out that $\gamma^*_{\rm TV}$ and $\gamma^*_{\rm TV}$ are proportional to changes in the angular momentum during the excitation process.[25] On the one hand, the thermal vortex is excited by heat from the unbinding of vortex–antivortex pair with $\hbar$ angular momentum because its characteristic perimeter is the de Broglie wavelength $\lambda_T=h/m^*v_T$ with thermal velocity v_T, which is universal for different materials; on the other

hand, the angular momentum of magnetic vortex excitation depends on the flip (i.e., twice) of the total spin of an ion in a strong field, which is $\hbar$ for Cu^{2+} (spin 1/2) and $4\hbar$ for Fe^{2+} (spin 2).[81] Therefore, the third inference is that $\gamma^*_{MV} = \gamma^*_{TV}$ for cuprates, but $\gamma^*_{MV} = 4\gamma^*_{TV}$ for iron-based HTSC. Indeed, we find that $\gamma^*_{MV} \approx \gamma^*_{TV} = 1.7 \pm 1$ for most cuprates (shown in Fig. 2(b) and Table 1), and $\gamma^*_{MV} \approx 4.4\gamma^*_{TV} = 7.5 \pm 1.5$ for BaFeAsP. This confirms the third inference that the thermal vortex state may be universal for HTSC compounds, and magnetic vortices are closely dependent on the iron's magnetic state, which is an intriguing effect worthy of further experimental and theoretical studies.

Table 1. Fitting parameters of Eq. (8) for quadrature MR. p is the corresponding carrier concentration, and x represents the doping levels for Sr or As in LSCO and BaFeAsP. ρ_I is the resistivity associated with impurity scattering, which is assumed to be as close to zero as possible. γ^*_{DW}, γ^*_{TV}, and γ^*_{MV} are scattering coefficients associated with DWO, thermal and magnetic vortices, respectively, which are fitted near the universal values (i.e., $\gamma^*_{DW} = 0.11 \pm 0.03$, $\gamma^*_{TV} \approx \gamma^*_{MV} = 1.7 \pm 0.4$) uncovered in our previous studies.[25,44] The effective mass m^* is estimated from previously reported experimental data.[57,60,67]

Compound	p or x	ρ_I ($\mu\Omega\cdot$cm)	γ^*_{DW}	γ^*_{TV}	γ^*_{MV}	m^* (m_e)
Bi-2201	0.12	0	0.11	1.1	1.3	2.7
Bi-2201	0.16	0	0.058	0.76	2.7	2.7
Bi-2201	0.18	0	0.077	0.62	1.3	2.7
LSCO	0.19	0	0.039	1.67	1.97	1.67
BaFeAsP	0.31	15.6	0.037	1.7	9.0	5.0
BaFeAsP	0.36	0	0.015	1.7	7.8	4.65
BaFeAsP	0.41	0	0.015	1.7	6.0	3.5

We conclude that these findings strongly support our proposal that the quadrature MR originates from the quantum coupling of three scattering channels of collective fluctuations rather than from the Lorentz force and macroscopic disorder.[24,82] Furthermore, combining the observations of Hayes *et al.* for optimal doping,[18] that of Ayres *et al.*[20] for over doping, and our result for underdoping described in the last subsection, we conclude that the quadrature MR is widespread with linear resistivity and must be an intrinsic property of the strongly correlated strange metal. The present work provides a unified description for this universal quadrature scaling.

5. Further predictions about scattering rate and other complex fluids

The above results exhibit the quantum coupling effects of multiple scattering channels in widespread resistivity scalings. On the other hand, these effects are initially indicated in the microscopic scattering rate, which ARPES experiments can examine directly. The most crucial prediction from Eq. (7) is that the NFL scattering rate in HTSC exhibits a unified quadrature coupling of temperature, magnetic field, energy, and the DWO scattering rate. First, we note that the asymptotic expression of this scaling at the DWO QCP ($\Gamma_Q = 0$) and zero-field limit equals Varma's phenomenological model of imaginary self-energy, $\mathrm{Im}\Sigma \propto \sqrt{(\pi k_B T)^2 + \hbar^2\omega^2}$,[51] consistent with ARPES measurements in both cuprate and iron-based HTSCs.[6,48,83] In addition, due to coupling with DWO ($\Gamma_Q \neq 0$), Eq. (7) predicts that the scattering rate of underdoped cuprate or iron-based HTSCs must exhibit a T-scaling crossover from quadratic to linear even at zero energy and field. Furthermore, it also predicts a linear-in-B dependence at high fields, low temperature, and energy. These two predictions are new from previous Fermi liquid or NFL theories and thus deserve direct examination by precise ARPES or optical conductivity measurements in underdoped and optimally doped HTSCs at both zero and high fields, respectively.

We also show that this NHH can be easily extended to other complex quantum fluids by specifying the corresponding symmetries. For the newly discovered bosonic strange metals in cuprates,[38] the transport carriers are spinless Cooper pairs (bosons) instead of spin-1/2 single electrons or holes (fermions). As a result, this bosonic strange metal's carrier scattering by thermal and magnetic vortices is spin-independent. It means that the anticommutation symmetry (i.e., Eq. (5)) of scattering matrices of the fermionic strange metal should be replaced by the commutation symmetry of one-by-one scattering matrices in this bosonic strange metal. Therefore, the MR of this bosonic strange metal should exhibit a linear summation of the linear-in T and B laws, which is highly consistent with Yang *et al.*'s experimental observations.[38] More importantly, this prediction indicates that quadrature and linear couplings of linear-in T and the linear-in B laws in MR distinguish the intrinsic spin nature of fermionic and bosonic strange metals, providing a clear answer to the present confusion about the origin of scaling diversity in HTSC MR.[19,82] Furthermore, it enables us to make an unexpected prediction about the strange metal of HTSCs; that is, by increasing temperature away from the superconducting critical temperature, the Cooper pairs break into spinor fermions, thus resulting in a spinor-symmetry constrained phase transition from the bosonic to fermionic strange metals. Interestingly, this prediction has been preliminarily observed in the high-field MR data of LSCO[18] since it exhibits linear and quadrature couplings at low and high temperatures, respectively. We thus suggest that experimentalists observe this phenomenon in more disordered compounds to uncover a novel phase transition form.

6. Discussion and conclusion

By extending the newly emerging comprehensive perspective (e.g., intertwined and vestigial orders[4,5]), this work develops a novel framework (the symmetry-constrained NHH) towards solving a long-lasting critical problem in correlated

electron systems: anomalous scalings of the NFL transport. These scalings have been widely observed in metallic states of HTSCs and heavy fermions. However, their quantum origin (especially the scattering mechanism) has been a long-standing issue. Physicists recently recognized that the main difficulty is a lack of theoretical methods that consider strong quantum fluctuations in the presence of abundant low-energy degrees of freedom.[8] This manuscript offers a novel solution by realizing that, in contrast to most theories considering one-fold scattering mechanism[7,21] and linear addition,[17,20] a comprehensive theory has to describe the quantum coupling of multiple scattering mechanisms. Here, by combining the newly emerging symmetry analysis of turbulence[37] and the NHH of open quantum dynamics,[35] we obtain a unified framework to quantify the quantum coupling of topological and non-topological (spin wave) excitations of mesoscopic orders. It comprehensively explains two widespread NFL behaviors (i.e., a temperature scaling crossover and the quadrature MR) in HTSCs or heavy fermions.

After going through some conceptual difficulties in familiarity with this phenomenology at the beginning, one can find that it may advance the understanding of the organizing principle of the NFLs in HTSC. In other words, this work uncovers the fundamental spinor symmetry constraint underlying NFL transport, enabling one to explain many transport anomalies from a unified perspective. For instance, the temperature scaling crossover and the quadrature MR in HTSCs result from the fermionic spinor's anticommutation symmetry. One may wonder how it relates to symmetry since quadrature scattering rate may be generated from a superposition of mutually orthogonal scattering channels. However, it is easy to prove that the orthogonality of these scattering channels requires anticommutation relations between their scattering matrices rather than their products equal to zero, which is the definition of vector orthogonality. The reason is that there are many non-zero scattering matrices (e.g., the combination of Pauli matrices $\sigma_i + \mathrm{i}\sigma_j$) whose squares equal to zero, which indicates that the zero product does not define the orthogonality of matrices. In contrast, if two matrices satisfy the anticommutation relation (i.e., Eq. (5)), the square of their summation equals the summation of their squares (i.e., $|\hat{K}_j + \hat{K}_k|^2 = \hat{K}_j^2 + \hat{K}_k^2$), which is a natural definition of orthogonality. In quantum physics, the fundamental origin of this anticommutation is the spin operator of the spin-$1/2$ fermions described by the Pauli or Dirac matrices.[50] Therefore, the spinor symmetry of fermions is a natural source of the orthogonality between scattering channels and the quadrature coupling of scattering rates. Therefore, some basic scattering mechanisms that can be mapped to fermionic spinor operators are anticommutative, and their coupling must be a quantum coupling represented by a quadrature coupling of scattering energy scales. Besides, we resolve that the different coupling types of magnetoresistance in bosonic and fermionic strange metals are due to their different spinor symmetry classes. Moreover, it enables us to predict an unexpected phase transition from the bosonic to fermionic strange metals by increasing temperature in HTSC compounds. Thus, demonstrating that symmetry determines the connection between NFL transport and order fluctuations may open up a new way to simplify the quantum transport theory of strongly correlated materials.

It is worth noting that the specific physical mechanism of different scattering types shown in Fig. 1 is also very critical for the anomalous transport of HTSCs. In previous works,[25,44] we have conducted a phenomenological analysis on the umklapp scattering by thermal and magnetic vortices and DWO fluctuations. It enables us to deduce an inverse square relation between the scattering rate and the characteristic length scale, i.e., Eq. (4), which much experimental data have verified. However, the microscopic description of these scattering mechanisms is still lacking, calling for further physical understanding and mathematical derivation. There also may be a query that since Eqs. (5)–(8) mainly focus on collective fluctuations in HTSCs, can the present model be extended to other correlated electron systems with different scattering mechanisms, e.g., magnetic impurities? The answer is positive since the fundamental contribution of this work is a unified NHH model for NFL transport (i.e., Eq. (1)) and the symmetry analysis (e.g., Eq. (5)) for the quantum coupling of multiple scattering mechanisms. Thus, this model can be extended to other complex fluids because of its proper decomposition for variations due to carriers and scattering mechanisms. Generally, we can treat three complexities: symmetry of the carrier (fermion or boson), spin- and momentum-dependence of the scattering mechanism (dependent or independent), the temperature, magnetic field, and frequency dependence of the scattering rate (linear or nonlinear). As discussed in Section 5, specifying these three aspects in Eqs. (5)–(8), our symmetry-constrained NHH model can potentially apply to other correlated electron systems.

To focus on discussing the impact of the quantum coupling of multichannel scattering, we only consider the energy and spin dependence of the scattering rates and neglect their momentum dependence. Moreover, we have assumed that the contribution of the band dispersion to resistivity can be renormalized to carrier density and effective mass. These assumptions are consistent with ARPES and angle-resolved MR measurements that the linear-in-T resistivity emerges mainly from a momentum-independent inelastic scattering rate.[40,84] Therefore, this work focuses on the ensemble-averaged (or macroscopic) transport behavior complementary to calculations for specific microscopic states of the elementary excitations by Zhao *et al.*[85] or Varma.[86] To describe complex be-

haviors (e.g., the anisotropy transport, the reconstructed Fermi surface, and the multiple-band effect), it is necessary to consider the specific band dispersion of elementary excitations and the momentum dependences of scattering rates. In other words, to extend our theory to higher-order physics, we could calculate the self-energy through a microscopic Hamiltonian or phenomenologically introduce the anisotropy of the scattering rate (such as in Ref. [13]), and it would be exciting to carry this out in the future. Although considering specific elementary excitations would be essential for clarifying microscopic physics, they would not affect our conclusion that symmetry is the fundamental constraint for the quantum coupling of multiple scattering channels.

The present work reveals that the quantum coupling of multiple scattering channels is the essential and intrinsic quantum nature of strongly correlated electrons. Thus, our theory is worthy of further experimental verification, theoretical derivation, and extension in three directions: first, it would be interesting to verify predictions about the scattering rate and resistivity (Eqs. (7) and (8)) for other strongly correlated materials, such as additional iron-based HTSC, iridate, organic, and heavy Fermion superconductors.[17,75,87,88] Primarily, we should further verify the scattering rate predicted with ARPES and optical conductivity data.[48,83,89] Through systematic quantification of the resistivity and the scattering rate, we will obtain the phase diagram for the evolution of each collective fluctuation, which will be very helpful in understanding the underlying electronic states.

Second, the present work provides insight into developing systematic theories for NFL transport in strongly correlated materials. Specifically, it suggests that, in contrast to Fermi liquids, the quantum coupling of multiple scattering channels in NFLs would result in systematic changes to transport theories, including Boltzmann equations and the Kubo formula. For the Boltzmann-equation simulation,[20] we suggest considering the momentum dependence of the universal scattering rate (Eq. (7)), combined with anisotropic electronic dispersion to simulate transport behaviors in HTSCs systematically. For instance, this could include the angle-resolved MR and the anomalous Hall effect of the strange metal phase.[13] These studies may advance the understanding of anomalous quadratic-T scaling of the inverse Hall angle and the origin of the violation of Kohler's rule. On the other hand, this work establishes a basis for developing a complete quantum transport theory of strongly correlated materials since it highlights the most critical degree of freedom (i.e., the spin degree of freedom) and the emergent symmetry (i.e., the anticommutation of scattering matrices), which may significantly simplify the number of degrees of freedom in the microscopic calculation. Specifically, we suggest that theorists calculate the microscopic formalism of the anti-Hermitian part $\mathrm{i}\hat{H}_{\mathrm{D}}$ in Eq. (1) and derive the universal scattering rate (Eq. (7)) from quantum field theory. These studies may significantly advance understanding the microscopic quantum origins of NFL transport, which is worthy of systematic efforts.

Finally, the present work highlights the fundamental symmetry constraint for NFLs and provides a novel theoretical framework (i.e., the symmetry-constrained NHH) to describe the phase transitions (dispersion and thermodynamics) and transport in correlated electron systems. In recently reported studies of NHHs,[35,36] it was found that the coupling between real energy dispersion and the finite lifetime may lead to the appearance of topological exceptional points and the existence of Fermi arcs, e.g., in heavy fermions. Similarly, we suggest combining our anti-Hermitian Hamiltonian $\mathrm{i}\hat{H}_{\mathrm{D}}$ for multichannel scattering by collective fluctuations with conventional Hermitian Hamiltonian $\hat{H}_0$ for symmetry-breaking orders to formulate a full description for the underlying quantum state (see Section I B in supplementary material for a simple NHH formulation of a typical propagator in the pseudogap phase). In this description, the present work points out that symmetry constraints provide a crucial clue to reducing the complexities of strong correlations. We believe this may enable us to resolve several critical problems associated with HTSCs and other strongly correlated materials, such as understanding the intertwined relationships among charge and spin orders, pseudogap, and superconductivity.

Acknowledgments

Project supported by the National Natural Science Foundation of China (Grant Nos. 91952201 and 11452002).

We thank Zheng-Yu Weng and Yi-Feng Yang for their constructive comments. We also thank Jian Wang, Dingping Li, Tao Li, and Ya-Yu Wang for the helpful discussions and Luhao Zhang for the help with manuscript preparation.

References

[1] Keimer B, Kivelson S A, Norman M R, Uchida S and Zaanen J 2015 *Nature* **518** 179
[2] Fernandes R M, Coldea A I, Ding H, Fisher I R, Hirschfeld P J and Kotliar G 2022 *Nature* **601** 35
[3] Wirth S and Steglich F 2016 *Nat. Rev. Mater.* **1** 16051
[4] Fradkin E, Kivelson S A and Tranquada J M 2015 *Rev. Mod. Phys.* **87** 457
[5] Fernandes R M, Orth P P and Schmalian J 2019 *Annu. Rev. Condens. Matter Phys.* **10** 133
[6] Varma C M 2020 *Rev. Mod. Phys.* **92** 031001
[7] Stewart G R 2001 *Rev. Mod. Phys.* **73** 797
[8] Lee S S 2018 *Annu. Rev. Condens. Matter Phys.* **9** 227
[9] Landau L D 1956 *Zh. Eksp. Teor. Fiz.* **30** 1058
[10] Landau L D 1957 *Sov. Phys. JETP* **32** 59
[11] Barišić N, Chan M K, Li Y, Yu G, Zhao X, Dressel M, Smontara A and Greven M 2013 *Proc. Natl. Acad. Sci. USA* **110** 12235
[12] Ando Y, Komiya S, Segawa K, Ono S and Kurita Y 2004 *Phys. Rev. Lett.* **93** 267001
[13] Hussey N E 2008 *J. Phys.: Condens. Matter* **20** 123201

[14] Analytis J G, Kuo H H, McDonald R D, Wartenbe M, Rourke P M C, Hussey N E and Fisher I R 2014 *Nat. Phys.* **10** 194
[15] Pelc D, Veit M J, Dorow C J, Ge Y, Barišić N and Greven M 2020 *Phys. Rev. B* **102** 075114
[16] Kasahara S, Shibauchi T, Hashimoto K, *et al.* 2010 *Phys. Rev. B* **81** 184519
[17] Licciardello S, Maksimovic N, Ayres J, Buhot J, Čulo M, Bryant B, Kasahara S, Matsuda Y, Shibauchi T, Nagarajan V, Analytis J G and Hussey N E 2019 *Phys. Rev. Research* **1** 023011
[18] Hayes I M, McDonald R D, Breznay N P, Helm T, Moll P J W, Wartenbe M, Shekhter A and Analytis J G 2016 *Nat. Phys.* **12** 916
[19] Giraldo-Gallo P, Galvis J A, Stegen Z, *et al.* 2018 *Science* **361** 479
[20] Ayres J, Berben M, Culo M, Hsu Y T, van Heumen E, Huang Y, Zaanen J, Kondo T, Takeuchi T, Cooper J R, Putzke C, Friedemann S, Carrington A and Hussey N E 2021 *Nature* **595** 661
[21] Maksimovic N, Hayes I M, Nagarajan V, Analytis J G, Koshelev A E, Singleton J, Lee Y and Schenkel T 2020 *Phys. Rev. X* **10** 041062
[22] Caprara S, Di C C, Seibold G and Grilli M 2017 *Phys. Rev. B* **95** 224511
[23] Miranda E and Dobrosavljević V 2005 *Rep. Prog. Phys.* **68** 2337
[24] Patel A A, McGreevy J, Arovas D P and Sachdev S 2018 *Phys. Rev. X* **8** 021049
[25] Li R and She Z S 2021 *New J. Phys.* **23** 043050
[26] Zaanen J 2004 *Nature* **430** 512
[27] Patel A A and Sachdev S 2019 *Phys. Rev. Lett.* **123** 066601
[28] Patel A A and Sachdev S 2017 *Proc. Natl. Acad. Sci. USA* **114** 1844
[29] Zaanen J 2019 *SciPost Phys.* **6** 061
[30] Anderson P W and Casey P A 2009 *Phys. Rev. B* **80** 094508
[31] Rice T M, Robinson N J and Tsvelik A M 2017 *Phys. Rev. B* **96** 220502
[32] Dai P 2015 *Rev. Mod. Phys.* **87** 855
[33] Chakravarty S, Laughlin R B, Morr D K and Nayak C 2001 *Phys. Rev. B* **63** 094503
[34] Datta S 2005 *Quantum Transport: Atom to Transistor* (New York: Cambridge University Press)
[35] Bergholtz E J, Budich J C and Kunst F K 2021 *Rev. Mod. Phys.* **93** 015005
[36] Nagai Y, Qi Y, Isobe H, Kozii V and Fu L 2020 *Phys. Rev. Lett.* **125** 227204
[37] She Z S, Chen X and Hussain F 2017 *J. Fluid Mech.* **827** 322
[38] Yang C, Liu H, Liu Y, *et al.* 2022 *Nature* **601** 205
[39] Krellner C, Lausberg S, Steppke A, Brando M, Pedrero L, Pfau H, Tencé S, Rosner H, Steglich F and Geibel C 2011 *New J. Phys.* **13** 103014
[40] Grissonnanche G, Fang Y, Legros A, Verret S, Laliberte F, Collignon C, Zhou J, Graf D, Goddard P A, Taillefer L and Ramshaw B J 2021 *Nature* **595** 667
[41] Fujita M, Hiraka H, Matsuda M, Matsuura M, Tranquada J M, Wakimoto S, Xu G Y and Yamada K 2012 *J. Phys. Soc. Jpn.* **81** 011007
[42] Frano A, Blanco-Canosa S, Keimer B and Birgeneau R J 2020 *J. Phys. Condens. Matter* **32** 374005
[43] Varma C M 2016 *Rep. Prog. Phys.* **79** 082501
[44] Li R and She Z S 2022 *Commun. Phys.* **5** 13
[45] Taillefer L 2009 *J. Phys. Condens. Matter* **21** 164212
[46] Peng Y Y, Huang E W, Fumagalli R, *et al.* 2018 *Phys. Rev. B* **98** 144507
[47] Arpaia R, Caprara S, Fumagalli R, *et al.* 2019 *Science* **365** 906
[48] Valla T, Fedorov A V, Johnson P D, Wells B O, Hulbert S L, Li Q, Gu G D and Koshizuka N 1999 *Science* **285** 2110
[49] Bruin J A N, Sakai H, Perry R S and Mackenzie A P 2013 *Science* **339** 804
[50] Dirac P A M 1928 *Proc. Roy. Soc. A* **117** 610
[51] Abrahams E and Varma C M 2000 *Proc. Nat. Acad. Sci. USA* **97** 5714
[52] Ando Y, Kurita Y, Komiya S, Ono S and Segawa K 2004 *Phys. Rev. Lett.* **92** 197001
[53] Padilla W J, Lee Y S, Dumm M, Blumberg G, Ono S, Segawa K, Komiya S, Ando Y and Basov D N 2005 *Phys. Rev. B* **72** 060511
[54] Nie L, Maharaj A V, Fradkin E and Kivelson S A 2017 *Phys. Rev. B* **96** 085142
[55] Yu B, Tabis W, Bialo I, Yakhou F, Brookes N B, Anderson Z, Tang Y, Yu G and Greven M 2020 *Phys. Rev. X* **10** 021059
[56] Anzai H, Ino A, Kamo T, Fujita T, Arita M, Namatame H, Taniguchi M, Fujimori A, Shen Z X, Ishikado M and Uchida S 2010 *Phys. Rev. Lett.* **105** 227002
[57] Dai Y M, Xu B, Cheng P, Luo H Q, Wen H H, Qiu X G and Lobo R P S M 2012 *Phys. Rev. B* **85** 092504
[58] Diao Z, Campanini D, Fang L, Kwok W K, Welp U and Rydh A 2016 *Phys. Rev. B* **93** 014509
[59] Zhou W and Liang W 1999 *Fundamental Research of High-Temperature Superconductor* (Shanghai: Shanghai Scientific and Technical Publisher)
[60] Ye Z R, Zhang Y, Chen F, Xu M, Ge Q Q, Jiang J, Xie B P and Feng D L 2012 *Phys. Rev. B* **86** 035136
[61] Mandrus D, Forro L, Kendziora C and Mihaly L 1991 *Phys. Rev. B* **44** 2418
[62] Ono S, Ando Y, Murayama T, Balakirev F F, Betts J B and Boebinger G S 2000 *Phys. Rev. Lett.* **85** 638
[63] Chen Y J, Lin P J, Wu K H, Rosenstein B, Luo C W, Juang J Y and Lin J Y 2013 *Supercond. Sci. Technol.* **26** 105029
[64] Casey P A and Anderson P W 2011 *Phys. Rev. Lett.* **106** 097002
[65] Tabiś W, Popčević P, Klebel-Knobloch B, Biało I, Kumar C M N, Vignolle B, Greven M and Barišić N 2021 arXiv: 2106.07457
[66] Zhang J, Ding Z, Tan C, Huang K, Bernal O O, Ho P C, Morris G D, Hillier A D, Biswas P K and Cottrell S P 2018 *Sci. Adv.* **4** eaao5235
[67] Spałek J, Zegrodnik M and Kaczmarczyk J 2017 *Phys. Rev. B* **95** 024506
[68] Barišić N, Badoux S, Chan M K, Dorow C J, Tabis W, Vignolle B, Yu G, Béard J, Zhao X, Proust C and Greven M 2013 *Nat. Phys.* **9** 761
[69] Hussey N E, Gordon-Moys H, Kokalj J and McKenzie R H 2013 *J. Phys.: Conf. Ser.* **449** 012004
[70] Li Y, Tabis W, Yu G, Barišić N and Greven M 2016 *Phys. Rev. Lett.* **117** 197001
[71] Peng Y Y, Fumagalli R, Ding Y, *et al.* 2018 *Nat. Mater.* **17** 697
[72] Kurashima K, Adachi T, Suzuki K M, Fukunaga Y, Kawamata T, Noji T, Miyasaka H, Watanabe I, Miyazaki M, Koda A, Kadono R and Koike Y 2018 *Phys. Rev. Lett.* **121** 057002
[73] Webb T A, Boyer M C, Yin Y, Chowdhury D, He Y, Kondo T, Takeuchi T, Ikuta H, Hudson E W, Hoffman J E and Hamidian M H 2019 *Phys. Rev. X* **9** 021021
[74] Fernandes R M, Chubukov A V and Schmalian J 2014 *Nat. Phys.* **10** 97
[75] Dai Y M, Miao H, Xing L Y, Wang X C, Wang P S, Xiao H, Qian T, Richard P, Qiu X G, Yu W, Jin C Q, Wang Z, Johnson P D, Homes C C and Ding H 2015 *Phys. Rev. X* **5** 031035
[76] Sefat A S, Singh D J, Jin R, McGuire M A, Sales B C and Mandrus D 2009 *Phys. Rev. B* **79** 024512
[77] Steppke A, Kuchler R, Lausberg S, Lengyel E, Steinke L, Borth R, Luhmann T, Krellner C, Nicklas M, Geibel C, Steglich F and Brando M 2013 *Science* **339** 933
[78] Wen H H, Mu G, Luo H, Yang H, Shan L, Ren C, Cheng P, Yan J and Fang L 2009 *Phys. Rev. Lett.* **103** 067002
[79] Comin R and Damascelli A 2016 *Annu. Rev. Condens. Matter Phys.* **7** 369
[80] Miao H, Fabbris G, Koch R J, *et al.* 2021 *NPJ Quantum Mater.* **6** 31
[81] Zhao Z X and Yu L 2013 *Fundamental Research of Iron-based Superconductors* (Shanghai: Shanghai Scientific and Technical Press)
[82] Boyd C and Phillips P W 2019 *Phys. Rev. B* **100** 155139
[83] Fink J, Rienks E D L, Yao M, *et al.* 2021 *Phys. Rev. B* **103** 155119
[84] Valla T, Fedorov A V, Johnson P D, Li Q and Koshizuka N 2000 *Phys. Rev. Lett.* **85** 828
[85] Zhao J Y, Chen S A, Zhang H K and Weng Z Y 2022 *Phys. Rev. X* **12** 011062
[86] Aji V, Shekhter A and Varma C M 2010 *Phys. Rev. B* **81** 064515
[87] Nakajima Y, Metz T, Eckberg C, *et al.* 2020 *Commun. Phys.* **3** 181
[88] Takahiro T, Kentaro K, Yoshiya U, Piers C and Satoru N 2015 *Science* **349** 506
[89] Prochaska L, Li X, Macfarland D C, Andrews A M, Bonta M, Bianco E F, Yazdi S, Schrenk W, Detz H, Limbeck A, Si Q, Ringe E, Strasser G, Kono J and Paschen S 2020 *Science* **367** 285